Agricultural and Forest Meteorology 249 (2018) 457–466

Contents lists available at ScienceDirect

Agricultural and Forest Meteorology

journal homepage: www.elsevier.com/locate/agrformet

Estimation of plant area index and phenological transition dates from digital repeat photography and radiometric approaches in a hardwood forest in the Northeastern United States

Motomu Toda[a,*], Andrew D. Richardson[b,c,d]

[a] Department of Environmental Dynamics and Management, Hiroshima University, Kagamiyama 1-7-1, Higashi-Hiroshima, 739-8521, Japan
[b] Department of Organismic and Evolutionary Biology, Harvard University, Cambridge, MA, 02138, USA
[c] School of Informatics, Computing and Cyber Systems, Northern Arizona University, Flagstaff, AZ 86011, USA
[d] Center for Ecosystem Science and Society, Northern Arizona University, Flagstaff, AZ 86011, USA

ARTICLE INFO

Keywords:
Phenology
Canopy cover imagery
Phenocam imagery
Radiometric PAR
Ameriflux network

ABSTRACT

Long-term, continuous digital camera imagery and tower-based radiometric monitoring were conducted at a representative hardwood forest site in the Northeastern United States, part of the AmeriFlux network. In this study, the phenological metrics of the leaf area index (LAI), plant area index (PAI) and associated transition dates (e.g., timing of the onset of leaf expansion and the cessation of leaf fall) were compared using 4-year of data from Bartlett Experimental Forest. We used digital repeat photography (DRP) imagery collected using two different methods ("canopy cover" and "phenocam" approaches), together with above- and below-canopy measurements of photosynthetically active radiation (PAR). The growth-period LAI estimated from canopy cover images (LAI_{CANOPY}) and the above and below canopy PAR measurements (LAI_{fPARt}) were within approximately the same range, in term of magnitude, as previous results for multiple comparative methods, although growing-season LAI_{CANOPY} was slightly lower ($3.11\ m^2\ m^{-2}$ to $3.35\ m^2\ m^{-2}$) than LAI_{fPARt} ($3.19\ m^2\ m^{-2}$ to $3.67\ m^2\ m^{-2}$). In addition, we derived phenological transition dates from PAI_{CANOPY}, PAI_{fPARt}, and color-based metrics calculated from the phenocam imagery (green (G_{CC}) and red (R_{CC}) chromatic coordinates). The transition dates in both spring and autumn differed somewhat according to method, presumably due to the vegetation status detection abilities of each vegetation metric. We found that LAI estimation from canopy cover images may be influenced by automatic exposure settings, which limits the ability to detect subtle changes in phenology during the transition phases in both spring and autumn. Particularly in autumn, the color-based metrics calculated from the phenocam imagery are decoupled from leaf area dynamics and thus PAI. While above and below canopy PAR measurements could yield the better indicators for estimating LAI, its seasonal dynamics, and associated phenological transition dates in long-term monitoring, we argue that there are obvious benefits to the multi-sensor approach used here.

1. Introduction

Plant phenology plays a fundamental role in regulating the seasonal dynamics of ecosystem function and structure, and hence the biogeochemical cycling of carbon and nutrients. Phenology also serves as an important control on energy and carbon exchanges via atmosphere–plant community interactions on local-to-global spatial scales (Richardson et al., 2013a). Thus, phenology drives the biological rhythms of the whole ecosystem under a given climate (Klosterman et al., 2014).

While phenology is sensitive to climate change, it is unclear how it will respond to future warming (Peñuelas et al., 2009). Several researchers have demonstrated the effect of climate change on phenology at an ecosystem scale over past decades and centuries (Ellwood et al., 2013; Primack, 2014). A comparison of recent phenophase measurements with phenology records, collected by hand at a small pond in Northeastern United States more than 15 decades ago by the American naturalist Henry D. Thoreau, revealed major interactive relationships between plants and animals as a result of the occurrence of phenological phases, such as earlier emergence of new leaves in spring that animals preferentially feed on (Ellwood et al., 2013; Primack and Gallinat, 2016). In contrast, several concerns have been raised regarding changes in phenology. For instance, what are the drivers of phenology in different ecosystems? Moreover, if future climate change

* Corresponding author.
E-mail addresses: todam@hiroshima-u.ac.jp (M. Toda), arichardson@oeb.harvard.edu, Andrew.Richardson@nau.edu (A.D. Richardson).

http://dx.doi.org/10.1016/j.agrformet.2017.09.004
Received 21 March 2017; Received in revised form 23 August 2017; Accepted 10 September 2017
Available online 19 September 2017
0168-1923/

induces changes in phenology, will this impair existing functioning, structure, and biogeochemical cycling in terrestrial ecosystems? A recent report on the relationship between climate change and phenology suggested that phenology might be less sensitive to increasing temperature than previously expected (Fu et al., 2015). However, this issue remains unresolved (Keenan, 2015).

Over the past decades, non-destructive optical or radiometric techniques, so-called "near-surface and remotely-sensed" approaches, have been used widely to evaluate plant phenology at various sites in the AmeriFlux network (e.g., Jenkins et al., 2007; Richardson et al., 2009; Ryu et al., 2010; Sonnentag et al., 2012). Instrument-based approaches can provide high-frequency, long-term data on phenology that are not subject to the inherent uncertainties and subjectivity of human observers (Richardson et al., 2013b). Several remote sensing approaches have been tested to monitor changes in phenological metrics or events, such as bud burst, leaf emergence, color, senescence and defoliation, in a range of terrestrial sites. Simple radiometric measurements − e.g. to quantify the total amount of light absorbed by or transmitted by the canopy − have been used to estimate the seasonality of leaf or foliage area (Turner et al., 2003; Richardson et al., 2012). Other approaches based on digital repeat photography (DRP) have also been applied. Specifically, imagery from upward-looking cameras has been used to quantify variation in canopy cover (Ryu et al., 2012), while imagery from downward-looking cameras has been used to quantify variation in canopy color (Richardson et al., 2007). Furthermore, advances in available satellite measurements have allowed us to assess spatial variability in phenology over a wider geographic range (Zhao et al., 2012; Klosterman et al., 2014).

While most instrument-based approaches are based on similar principles (i.e., quantifying how light is processed by the canopy, and how this changes seasonally), they each have individual advantages that allow them to capture unique changes or fine differences in phenology. Photosynthetically active radiation (PAR, 400–700 nm), is absorbed, scattered, and transmitted by plant foliage (as well as woody stems and branches). Broadband radiometric measurements of PAR permit optically-based estimates of leaf or foliage area using the fraction of light transmitted through the canopy. Specifically, in forests with spatially homogeneous foliage arrangement, the gap fraction principle enables accurate assessment of leaf area from a single set of above- and below-canopy measurements. However, more commonly, especially in naturally regenerated or unmanaged forests, the ideal spatial characteristics are rarely achived, The resulting heterogeneous forest structure then requires the deployment of, multiple sensors within the forest to mitigate the effects of spatially heterogeneous below-canopy light environment on the evaluation of foliage area (Jenkins et al., 2007).

Meanwhile, the DRP approach has been shown to be applicable in various tower-flux operation sites across the world because of its user-friendly and weatherproof features (ex., Ryu et al., 2010; Keenan et al., 2014; Zhao et al., 2012; Ma et al., 2014; Toomey et al., 2015; Linkosalmi et al., 2016 Moore et al., 2017). Software tools and methods for processing imagery taken using DRP have been specifically designed to track phenolgy (ex., Leblanc, 2004; Macfarlane et al., 2007; Richardson et al., 2007; Ide and Oguma, 2010; Sonnnentag et al., 2012). With upward-looking camera imagery (e.g., canopy cover photography), the extracted field of view is typically somewhat narrow, and therefore the use of multiple cameras may be desirable to accurately capture spatial heterogeneity (Ryu et al., 2010). For example, in savanna ecosystems where sparsely distributed trees mix with grass, there is a particularly high degree of spatial heterogeneity but longterm canopy cover DRP measurements tracked successfully seasonal and annual variability in vegetation indices such as leaf or foliage area in these ecosystems (Ryu et al., 2012; Ma et al., 2014 Moore et al., 2017). On the other hand, the application to the foliage area evaluation from the corresponding DRP approach in the forests with dense canopy closure has still remained under investigation (Ryu et al., 2012; Macfarlane et al., 2014). In temperate deciduous forests, during the full-leaf period, a scene from the canopy cover DRP approach gets darker due to light occlusion by foliage above the dense canopy. To brighten the image, a digital camera set to automatic exposure will then increase the exposure time or the diameter of the aperture, similar to the process performed for human eye (Macfarlane et al., 2014). It has been acknowledged that as a result, many pixels, including small gaps between leaves, twigs and small branches in dense canopy, might be masked by these exposure effects, leading to underestimation of the maximum foliage area from longterm DRP measurements with automatic exposure setting.

To detect phenology using vegetation metrics of interest, the simultaneous application of multiple near-surface remote sensing approaches has been conducted (Zhao et al., 2011). Previous research has mainly focused on leaf area index (LAI), because this is essential for representing the overall function, structure, and resultant diversity of ecosystems via their photosynthetic activity. However, what is actually measured is plant area index (PAI), representing the aggregated leaf and woody plant materials, such as stems, twigs, and fine branches (Macfarlane et al., 2007; Zhao et al., 2011). The PAI is directly calculated from canopy cover images (PAI_{CANOPY}) and above- and below-canopy PAR measurements by which the fractional PAR transmitted through the canopy (fPARt) can be obtained (PAI_{fPARt}). PAI can be also converted into LAI in conjunction with direct sampling technique using litter-trap observations. Another approach to convert PAI to LAI is to subtract off the dormant-season PAI because this represents only woody material. Therefore, PAI might be a beneficial metric when these different approaches are compared in the corresponding time series.

As an additional metric of interest, we focus on the phenological transition dates. The transition dates indicate the phenologic timing associated with specific leaf or foliage developmental phases. Particularly, it is significant to obtain accurate evaluation of the annual difference in these timings in spring and autumn periods for deciduous forests as changes in the phenologic timing have a great potential to alter the whole biological rhythm in the ecosystem over decadal time scales in response to future climate change (Primack and Gallinat, 2016). For the purpose of evaluating the phenologic transition dates, we used the time series data of PAI_{CANOPY} and PAI_{fPARt}, and the green and red chromatic coordinates derived from phenocam imagery (green (G_{CC}) and red (R_{CC}) chromatic coordinates). The phenocam DRP approach captures an oblique view of the canopy from the digital camera mounted on a viewpoint above the canopy, serving as valuable ground truth validation data for satellite remote sensing phenology data products (Klosterman et al., 2014; Ma et al., 2014). The vegetation metrics G_{CC} and R_{CC} from the phenocam DRP approach are calculated from the ratio of green and red digital number (DN) within each image. Changes in these metrics may reflect physiological (or functional) and physical (or structural) characteristics of foliage. Accordingly, phenological metrics derived based on canopy color variations may differ from those based on the structural metric of PAI because canopy color depends on both the amount of leaf area and the color of individual leaves (Keenan et al., 2014).

In this study, we compare the phenologic metrics derived from different near-surface remote-sensing approaches using four years of data (2013–2016) from a temperate deciduous forest. We examine the vegetation features detectable from these and we explore the potential for individual methods to determine the same parameter of interest. Specifically, we compare start- and end-of-season transition dates estimated from light interception from fractional PAR measurements, foliage cover from digital upward-pointing canopy cover images, and greenness from oblique canopy view images.

2. Site information

Field observations were conducted in the Bartlett Experimental Forest (44°3′52.7″N, 71°17′17.1″W, 270 m a.s.l), located in the lowlands

of the White Mountains, New Hampshire, USA. The forest was mainly composed of red maple (*Acer rubrum*, 28% of basal area), American beech (*Fagus grandifolia*, 20%), and other hardwood species, such as sugar maple (*Acer saccharum*), paper and yellow birch (*Betula papyrifera* and *B. alleghaniensis*), and aspen (*Populus grandidentata*) (31%), and also included the conifers eastern hemlock (*Tsuga canadensis*, 17%) and eastern white pine (*Pinus strobus*, 4%). The central aim of the field campaigns is to determine the interannual variability in energy and CO_2 exchange between the atmosphere and forest ecosystem comprising the representative tree species using a fast response eddy covariance technique system with a 26.5-m-high flux tower, which has been operated as an AmeriFlux monitoring network site since 2004 (Jenkins et al., 2007). In recent years, several extreme weather events have occurred in the New England region surrounding the study site. For instance in 2010, an unusually warm spring with temperatures 3 °C above normal was followed by a severe frost event that damaged newly-emerged leaves (Hufkens et al., 2012). Moreover, in the summer of 2016, July-September temperatures across the region were the second warmest on record, while precipitation was substantially below normal. This led to moderate-to-severe drought conditions (http://droughtmonitor.unl.edu/), which may have influenced canopy development and/or the amount of foliage maintained during the summer months.

3. Database for deriving the PAI and phenological transition dates

3.1. Procedures to estimate PAI from canopy cover images

3.1.1. Camera setting and image selection

We collected fisheye images to investigate the overall phenological dynamics of the forest canopy using a portable time lapse camera (WCT01-00114; Wingscapes, Alabaster, AL, USA.), with fisheye conversion lens (Gyorome 8; FIT, Fukuoka, Japan) to compensate for the fact that the camera's native field of view was slightly narrower than typically used in digital cover photography applications (Zhao et al., 2012). The camera was mounted with an upward-pointed lens at a height of 1.5 m above the forest floor, about 20 m to the north of the AmeriFlux tower. Every digital image was recorded in high–quality (2592 × 1944 pixels) JPEG format. The camera's focus was set to infinity, and aperture (F-value) was fixed as F/2.8. Accordingly, exposure time for shooting changed automatically depending on the canopy status. Exposure time was shortest (1/800 s) during the leafless period, and longest (1/30 ~ 1/40 s) during the summertime period of peak PAI. Images were taken hourly from mid-March to the end of November from 2013 to 2016. The camera used in this study had the advantages of being inexpensive and weatherproof with a long battery life, allowing it to record camera images continuously in a remote site that was difficult to visit at regular intervals.

For image processing, we converted the standard fisheye images into rectangular images by cropping the fisheye images to focus on phenological variations in the intermediate and upper canopy layers in the center of the images. Images were cropped to obtain the maximum possible width and height from the center point beforehand using the freeware image-processing computer program, GIMP 2.8 (GNU image manipulation program; www.gimp.org), while removing any black pixels in outer-edge of the original fisheye images. All images used in the analysis were processed in the same manner (Fig. 1)

3.1.2. Image pixel classification

We applied a series of automated procedures for pixel classification to identify foliage, between-crown small gaps, and large gaps in each image using a MATLAB (The Mathworks Inc., MA, USA) algorithm developed by Macfarlane (2011). Firstly, an attempt was made to classify pixels of each image into either vegetation canopy or other sky element by using the histogram of the blue band channel in the range from 0 to 255 of digital number (DN) for all pixels of each image (Leblanc et al., 2005), and the corner-detection method was applied to

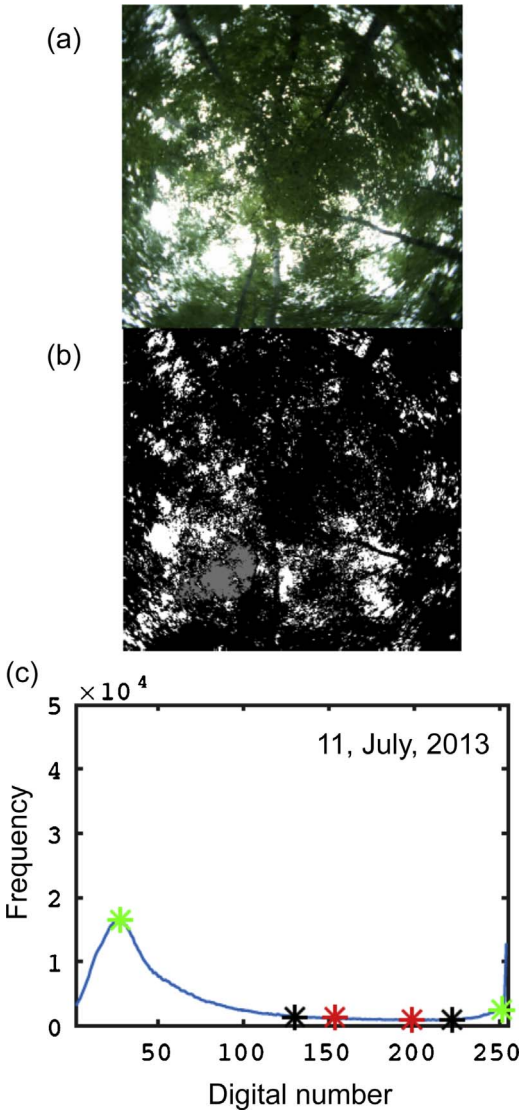

Fig. 1. A view of the upper canopy from canopy cover images taken on 22 July 2013 using an upward-pointed digital camera in the Bartlett Experimental Forest. The image is converted into grey-scale binary images (middle part) using image analysis developed by Macfarlane (2011). Additionally, image is separated into three parts: grey designates the large gaps between crowns in the overstory trees, black designates the foliage, and white designates the small gaps within the crown. The lower part indicates the frequency of color histogram of the blue band channel in the image. The two green asterisks indicate the maximum of canopy crown (left-hand side) and sky/cloud (right-hand side) pixels, respectively. Black asterisks indicate the boundary of each of canopy crown and sky elements determined using the modified corner detection method: the lower is right-sided of the range of canopy crown, and higher is left-sided of the range of sky element. Red asterisks indicate the final boundary of canopy and sky elements determined from the dual binary method: the lower is right-sided of the range of canopy crown, and higher is left-sided of the range of sky element. (For interpretation of the references to colour in this figure legend, the reader is referred to the web version of this article.)

identify two representatives of boundary for the vegetation and sky elements (Macfarlane, 2011). There are found maxima in the lower and higher channels for canopy ($DN_{MAX,CANOPY}$) and sky ($DN_{MAX,SKY}$) elements, respectively (Fig. 1), and these maximum DNs are in the range of $DN_{L1} < DN < DN_{L2}$ for canopy, and $DN_{R1} < DN < DN_{R2}$ for sky, where $DN_{L1} = 5$, $DN_{L2} = 25$, $DN_{R1} = 200$, and $DN_{R2} = 250$ were assumed as an initial conditions.

As the numerical exploration of MATLAB algorithm used, the maxima of DN for canopy and sky are determined if they satisfies the following:

$$DN_{L2} - DN_{MAX,CANOPY} \geq 10 or DN_{MAX,SKY} - DN_{R1} \geq 10 \quad (1)$$

If not satisfied, further exploration are continued until these evaluation completed successfully using an alternative window of DN as follows:

$$DN_{L2} = DN_{L2} + 25 and/or DN_{R1} = DN_{R1} - 25 \quad (2)$$

The next step is to evaluate the right side edge of lower maximum for vegetation canopy (DN_{LC}) and the left side edge of higher maximum for sky elements (DN_{UC}) in the blue channel. These can be explored by finding the point of maximum curvature on the L-shaped curves in the histogram by fitting a straight line from the maxima bin for canopy and sky to the last non-empty bin, respectively (Macfarlane, 2011). In the process, Macfarlane (2011) modified the original corner detection method proposed by Rosin (2001), in which the terminal of the straight fitting line on the DN_{MAX} for canopy and sky has been set to the mean number of pixels per bin for the whole image so that the slope of straight lines has been obtained, thereby DN_{LC} and DN_{UC} were determined in this study (they represents black asterisks in the lowest part in Fig. 1).

In addition, the pixels in the intermediate range between these boundaries DNs (DN_{LC} and DN_{UC}) are referred to as mixed pixels (Macfarlane, 2011). We used dual binary threshold that separates the mixed pixels into either vegetation canopy or sky element unambiguously using DN_{LC} and DN_{UC} obtained in the prior process following the same procedures as Macfarlane (2011). In this, pixels in $DN < DN_{LC}$ were initially classified as foliage and gaps smaller than 0.01% of the image size. In addition, we assumed a 25% threshold to minimize the loss of small gaps between-crown, which is given as $DN_{LC} + (DN_{UC} - DN_{LC})$ x 0.25. While, a 75% threshold, which is given as $DN_{LC} + (DN_{UC} - DN_{LC})$ x 0.75, was applied to the remainder of the image to minimize classifying foliage as sky in brighter ranges. Details on the pixel classification process are described in Macfarlane (2011) and Ryu et al. (2012).

We used additional procedures to identify high-quality canopy cover images and to construct a time series of the estimated PAI. The imagery was archived at 1 h interval from 4:00 a.m. to 21:00 p.m. Underexposed images recorded before sunrise or after sunset were excluded. Furthermore, we selected images for the analysis by visually examining all images and excluding those that, for example, included intensive solar illumination in the cropped field of view, had dew or raindrops on the plastic camera dome, or that appeared to have been recorded under mixed sun/cloud conditions. Ultimately, 500 images were selected from among the 4649 available images in 2013, 586 from among 4085 in 2014, 548 from among 5050 in 2015, and 218 from among 4302 in 2016. It should be noted that, for a variety of reasons including low batteries, operator error, and system failure, the camera did not record images for the following periods: 7 October–7 November in 2015, and 19–29 April 2016, and 20 September onward in 2016.

3.1.3. PAI estimation from canopy cover images

Based on the pixel classifications described above, the PAI from a canopy cover image (PAI_{CANOPY}) can be calculated by an inversion of Beer's law as follows:

$$PAI_{CANOPY} = -f_c \ln(\phi)/k \quad (3)$$

where f_C is the fraction of crown cover as the fraction of the sum of foliage (f_F) and small gaps within crown. & x3D5; is the gap within the crown envelopes, referred to as crown porosity (Kucharik et al., 1999; Macfarlane et al., 2007; Pekin and Macfarlane, 2009). k (= G(θ)/cos(θ) where G is the foliage projection function, and θ is a zenith angle) is the light extinction coefficient; we assumed that k = 0.5 for all images, which is a widely used assumption (e.g., Macfarlane et al., 2007), since it is difficult to estimate k (Chianucci and Cutini, 2013) without additional measurements (Ryu et al., 2012). & x3D5; is given as follows:

$$\phi = 1 - \frac{f_F}{f_C} \quad (4)$$

Eq. (4) can be substituted using the fraction of the total gap (f_G), the fraction of the sum of small within-crown and large between-crown gaps in the image to yield:

$$\phi = 1 - \frac{(1 - f_G)}{f_C} \quad (4)'$$

In this study, it is defined that the large gap is equivalent to a lump of pixels > 1.3% of the total pixels in the image.

3.2. Estimation of PAI from multiple PAR measurements

PAI was also evaluated from a suite of quantum sensors (model 190SA; Li-Cor, Lincoln, NE, USA) (Jenkins et al., 2007). One PAR sensor was mounted at a height of 25 m on the 26.5 m high flux tower to capture the incident PAR (Q_0). Four PAR sensors were placed 1-m above the ground (and above the understory) in a circle (radius of 15 m) centered at the tower, to capture the representative transmitted radiation component (Q_t). Using the radiation components, the fraction of PAR radiation transmitted through the canopy (fPARt) was calculated as follows (Richardson et al., 2013b):

$$fPARt = Q_t/Q_0 \quad (5)$$

where Q_t is the mean of the four quantum sensor measurements. PAI estimated from fPARt, (PAI_{fPARt}), can be expressed as:

$$PAI_{fPARt} = -ln(fPARt)/k' \quad (6)$$

where k' (= G(θ')/cos(θ')) is the light extinction coefficient for the corresponding approach, but with a particular solar zenith angle θ'. To reduce the effects of seasonality in the solar elevation, only two fPARt data points on the day when θ' was closest to 57° were used, averaged from the available continuous hourly PAR measurements, and considering that, when θ' = 57°, all leaf inclination distribution functions converge and G (57) is identical to 0.5 (Richardson et al., 2013b; Keenan et al., 2014). θ' was calculated based on site longitude and latitude information, time of day, and day of year using the Solar Position Calculator designed by NOAA Earth System Research Laboratory (ESRL) (https://www.esrl.noaa.gov/gmd/grad/solcalc/azel.html). Using data from a co-located sunshine sensor (model BF3; Delta-T Devices Ltd., Cambridge, UK), we further screened data to exclude observations where the PAR diffuse fraction (PARdiff/Q_0) was < 0.8.

3.3. Derivation of LAI from the estimated PAI

LAI is evaluated using the PAI measurements alone derived from the optical devices, by subtracting the averaged PAI during leafless period (an estimate of WAI, representing woody material) from the actually measured PAI throughout a year (i.e., LAI = PAI-WAI). We did not account for the reduced effects of woody materials overlapped by leaves in the leafy period, by which the contribution of WAI might be over-estimated during the growing season (Kucharik et al., 1998; Ryu et al., 2012). We determined the winter duration by integrating the following periods from 1 March to the start of leaf emergence in spring, and the leaf fall completion in autumn to 30 November, where the specific dates of the start of leaf emergence in spring and the leaf fall completion in autumn were identical to SOS and EOA that are referred in the section 3.5. During the 4-year studied period, there was no major change in WAI. The winter period PAI was 0.52 ± 0.06 $m^2 m^{-2}$ (mean ± s.d.) for canopy cover images, and 0.98 ± 0.30 $m^2 m^{-2}$ for radiometric PAR measurements, respectively (Note that the dates of EOA in 2015 and 2016 from the DRP approach were not obtained because of the camera operation failure, and the last date during the plant growth period in which the maximum PAI sustained was assigned). Accordingly, we used these PAI values as the winter baseline to convert PAI to LAI during leafy period. This processing does not affect the timing of the phenophase transitions, and thus it does allow for more direct comparison between LAIs derived from canopy cover images

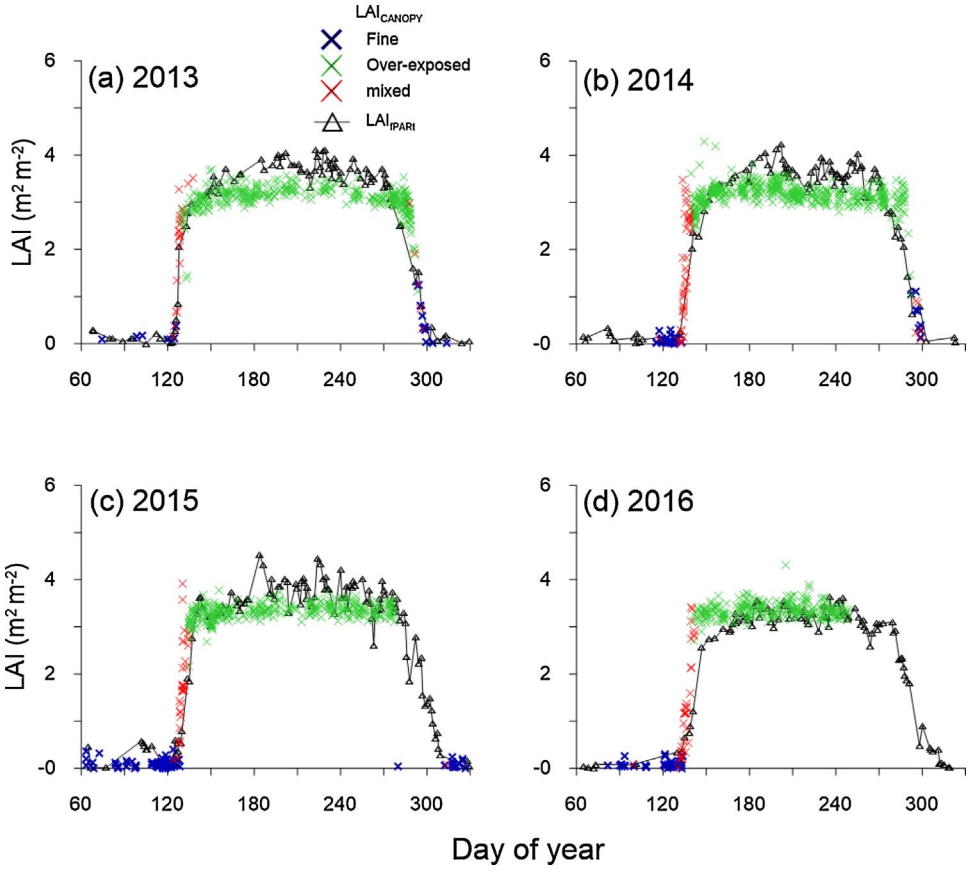

Fig. 2. Seasonal variation in leaf area index (LAI) in each of the four study years (a–d) 2013–2016. The crosses denote the LAI detected from the digital canopy cover images (LAI_{CANOPY}), and the different colors represent the image condition or quality based on the digital image processing designed method of Macfarlane (2011). Here, blue represents a fine image, green represents an overexposed image, red represents an image with many mixed pixels (composed of both canopy crown and sky), and magenta represents an image with ambiguous separation between canopy crown and sky elements. The solid black line with triangles shows the LAI calculated from above and below canopy photosynthetic active radiation (PAR) measurements (LAI_{fPARt}). (For interpretation of the references to colour in this figure legend, the reader is referred to the web version of this article.)

(LAI_{CANOPY}) and from radiometric PAR measurements (LAI_{fPARt}).

3.4. Use of additional VIs and green and red chromatic coordinates

To complement the above estimates of PAI, we used data from a networked digital camera (model 211; Axis Communications, Lund, Sweden), mounted on the tower at a height of 26 m since 2005. This phenocam is pointed north and angled downward at 20° below horizontal, so as to obtain an oblique view of the canopy (See Richardson et al. (2007, 2009) for phenocam images used in the current study). Image processing consisted of defining a region of interest (here, trees in the immediate foreground of the image, corresponding approximately to the field of view of the upward-looking hemispherical camera used for PAI_{CANOPY}) and then calculating the mean intensity (digital number, DN) for each color channel (i.e. R_{DN}, G_{DN}, and B_{DN}, for red, green and blue, respectively) across this region. From this we then calculated two widely-used indices to characterize canopy color, the green chromatic coordinate (G_{CC}) and red chromatic coordinate (R_{CC}) (Sonnentag et al., 2012):

$$G_{CC} = \frac{G_{DN}}{R_{DN} + G_{DN} + B_{DN}}; R_{CC} = \frac{R_{DN}}{R_{DN} + G_{DN} + B_{DN}} \quad (7)$$

We used the 90th percentiles *of* G_{CC} (G_{CC}_90) and R_{CC} (R_{CC}_90) in 3-day moving windows (Sonnentag et al., 2012; Toomey et al., 2015) to minimize the impact of variation in lighting and weather conditions.

3.5. Derivation of the transition dates in spring and autumn

To explore the phenological transition dates in spring and autumn, we applied a simple sigmoid function to the VI time series data (Klosterman et al., 2014), described as follows:

$$y(t) = \frac{c}{1 + \exp(a + bt)} + d \quad (8)$$

where y(t) presents the estimated VI at time t. In this study, we used PAI_{CANOPY}, PAI_{fPARt}, and G_{CC} as VIs to determine the transition dates in spring. In addition to these three VIs, R_{CC} was used to determine the transition dates in autumn. *a* and *b* are fit parameters that control the timing and rate of increase (or decrease) of the sigmoid curve, i.e. the start of greening in spring (SOS) and senescence in autumn (SOA), the end of the completion of leaf unfolding (EOS) and leaf falling (EOA), and the length from onset to maturity of phenologic phase in spring and autumn, respectively. *c* is the amplitude of VI, and *d* the baseline value; therefore, the sum of *c* and *d* indicates the maximum VI value. These optimum parameters are determined by fitting the observed VI using a non-linear regression approach for both spring and autumn within a year. Start and end of season transition dates were determined as the maximum values of the rate of curvature of y(t), while the maximum rate of change (corresponding to the minimum value of the rate of curvature of y(t)) in VI is defined as the middle of the phenological transition period in spring (MOS) and in autumn (MOA) (Zhang et al., 2003). In contrast to the seasonal patterns of PAI_{CANOPY}, and PAI_{fPARt}, and G_{CC}, which rise in spring, flatten off in summer, and decline in autumn, the R_{CC} signal rises to separate peaks in spring and autumn. Here we focus on the autumn peak, which corresponds to the development of autumn colors (predominantly reds and oranges), particularly in red maple and sugar maple. Accordingly, we established MOA as the date when the maximum R_{CC} was obtained, and determined SOA by fitting Eq. (8) in the period before MOA, and EOA in the period after MOA. Alternatively, for estimating the EOA dates from R_{CC} time series data in autumn, Klosterman et al. (2014) used smoothing and interpolation method. In the processing, R_{CC} data were first smoothed using the local regression (loess) algorithm (they used loess algorithm in MATLAB) that moderates any noise by estimating a particular local regression to a second-order polynominal at each point in R_{CC} data

Table 1
Summary of the phenological transition dates from 2013 to 2016 derived form the vegetation indices (VIs) of (a) PAI derived from digital canopy crown cover imagery (PAI_{CANOPY}), (b) PAI derived from above and below canopy PAR measurements (PAI_{fPARt}), (c) 90th percentile of greenness for a 3-day moving window processing window derived from digital landscape imagery (G_{CC}_90), and (d) the 90th percentile of redness for a 3-day moving processing window redness derived from digital landscape imagery (R_{CC}_90). In the Table 1, the EOA dates from R_{CC}_90, which are enclosed in bracket, were estimated from the smoothing and interpolation approach using the loess algorithm in the free software R. The transition length represents the difference in dates between EOS and SOS for the spring, and between EOA and SOA for the autumn phenological phases. Note that the dates used each denote day of year (DOY).

Vegetation index	Year	SOS	MOS	EOS	Transition period	Year	SOA	MOA	EOA	Transition period
(a) Canopy cover imagery	2013	123	126	129	6	2013	287	293	298	11
	2014	131	136	142	11	2014	287	291	295	8
	2015	126	130	132	6	2015	–	–	–	–
	2016	132	137	142	10	2016	–	–	–	–
(b) fPARt	2013	124	128	136	12	2013	273	290	303	30
	2014	128	140	149	21	2014	271	287	303	32
	2015	127	134	140	13	2015	279	293	314	35
	2016	131	141	152	21	2016	279	291	306	27
(c) G_{CC}_90	2013	119	131	140	21	2013	251	266	278	27
	2014	128	137	143	15	2014	248	263	278	30
	2015	125	131	137	12	2015	260	272	284	24
	2016	131	137	146	15	2016	251	269	284	33
(d) R_{CC}_90						2013	254	275	293 (299)	39 (45)
						2014	254	272	299 (308)	45 (54)
						2015	260	287	- (311)	- (51)
						2016	–	284	- (311)	- (−)

used. In this study, we applied the method for estimating EOA from R_{CC}_90 data using loess algorithm in the freeware program for statistical computing and graphics, R (www.r-project.org), and all of R_{CC}_90 data in autumn were used for the regression. In the processing, we set the fraction of annual data (f) in the loess algorithm, which is indispensable for giving beforehand to $f = 0.15$.

4. Results

4.1. Annual variations in LAI

The LAI_{CANOPY} was non-zero but nearly constant before leaf appearance in spring and after all leaves fell in autumn, which was attributed to the fact that most images were taken under appropriate exposure conditions (see the blue-colored cross in Fig. 2). During foliage development, LAI_{CANOPY} increased sharply in spring while during senescence LAI_{CANOPY} similarly decreased sharply in autumn (see the red-colored cross in Fig. 2; Table 1). During the growth period, the maximum values of LAI_{CANOPY} (green-colored cross) varied within a narrow range among the four study years ($3.11 \pm 0.24\ m^2\ m^{-2}$ (mean ± s.d.) in 2013, $3.19 \pm 0.19\ m^2\ m^{-2}$ in 2014, $3.31 \pm 0.20\ m^2\ m^{-2}$ in 2015, and $3.35 \pm 0.16\ m^2\ m^{-2}$ in 2016). These values were averages of the LAI_{CANOPY} time series data between EOS and SOA (Details on EOS and SOA are given in section 4.2 and Table 1, please note that we used the last date during the growing period instead of EOA in 2015 and 2016). On the other hand, LAI_{fPARt} was marginally more variable than LAI_{CANOPY} during the dormant season. The maximum values of LAI_{fPARt} were greater than those of LAI_{CANOPY}, and had greater interday variability (Fig. 2), reflecting the dual effects of heterogeneous cloud distribution on the above-canopy PAR measurements, and of heterogeneous canopy structure on the below canopy PAR measurements. The averaged maximum LAI_{fPARt} was $3.53 \pm 0.33\ m^2\ m^{-2}$ during the growing season ($3.65 \pm 0.24\ m^2\ m^{-2}$ in 2013, $3.60 \pm 0.25\ m^2\ m^{-2}$ in 2014, $3.67 \pm 0.33\ m^2\ m^{-2}$ in 2015 and $3.19 \pm 0.22\ m^2\ m^{-2}$ in 2016), which was the average of the time series LAI_{fPARt} data between EOS and SOA. Therefore, the difference in LAI_{CANOPY} and LAI_{fPARt} was found at most $0.30\ m^2\ m^{-2}$ on average. In 2016, LAI_{CANOPY} was comparable to those from the other 3 years. Contrastingly, LAI_{fPARt} in 2016 decreased by $0.45\ m^2\ m^{-2}$ on average compared to the other 3 years ($P < 0.001$). Whether or not the decrease reflected the direct impact of abnormal drought event during summer of 2016 on leaf area is unknown. Overall, however, LAI from the two approaches was consistent to within $0.5\ m^2\ m^{-2}$ across the 4 years of study.

4.2. Phenological transition dates

Figs. 3 and 4 show the transition dates in spring and autumn, respectively. In this processing, the time series of PAI_{CANOPY} and PAI_{fPARt} derived from canopy cover images and radiometric PAR measurements directly were used to identify the transition dates, together with the additional VIs of G_{CC}_90 in spring, and of G_{CC}_90 and R_{CC}_90 in autumn. These figures show the minimum and maximum rates of change in curvature, from which the transition dates were determined without setting thresholds or using empirical constants (Zhang et al., 2003). In addition, Table 1 lists the six determined transition dates.

For PAI_{CANOPY}, PAI_{fPARt}, and G_{CC}_90, the dates of SOS were in reasonably close agreement, and the interannual patterns were similar (2013 was the earliest SOS and 2016 the latest) (Table 1). SOS from G_{CC}_90 occurred about a few days ahead of that from PAI_{CANOPY} on the 4-year average, which was almost the same as PAI_{fPARt}. However, because the transition from SOS to EOS occurred much faster (≈1 week) for PAI_{CANOPY} than either PAI_{fPARt} (≈2 weeks) or G_{CC} (≈2 weeks), EOS dates were not in good agreement among any of the methods (Table 1), and the patterns of interannual variability in EOS were less consistent among methods. Overall, EOS from PAI_{CANOPY} occurred about 5 days ahead of that from G_{CC}_90 but 8 days ahead of that from PAI_{fPARt}.

For the autumn phenology, the SOA dates from PAI_{CANOPY} were 1 or 2 weeks behind from PAI_{fPARt}, whereas the SOA dates of G_{CC}_90 and R_{CC}_90 occurred much earlier (≈DOY 250). Conversely, the EOA dates from G_{CC}_90 occurred much earlier than those from PAI_{CANOPY} and PAI_{fPARt} (≈2-3 weeks). The EOA dates from R_{CC}_90 using the sigmoid function of Eq. (8) were similar to PAR_{fPARt} in 2013 and 2014 (DOY 293 for 2013 and DOY = 299 for 2014), while the method failed to detect EOA dates in 2015 and 2016. The advantage of use of sigmoid function was to be capable of determining the transition date without setting thresholds or using empirical constants. However, the failure for detecting the EOA dates in 2015 and 2016 indicates potential limitations to this approach (Fig. 4, Table 1). In contrast, an alternative approach to estimate EOA in autumn, smoothing and interpolation method detected the similar EOA dates compared to those from PAI_{fPARt} from 2013 to 2015 (Fig. 4, Table 1). For all indices, the interannual patterns

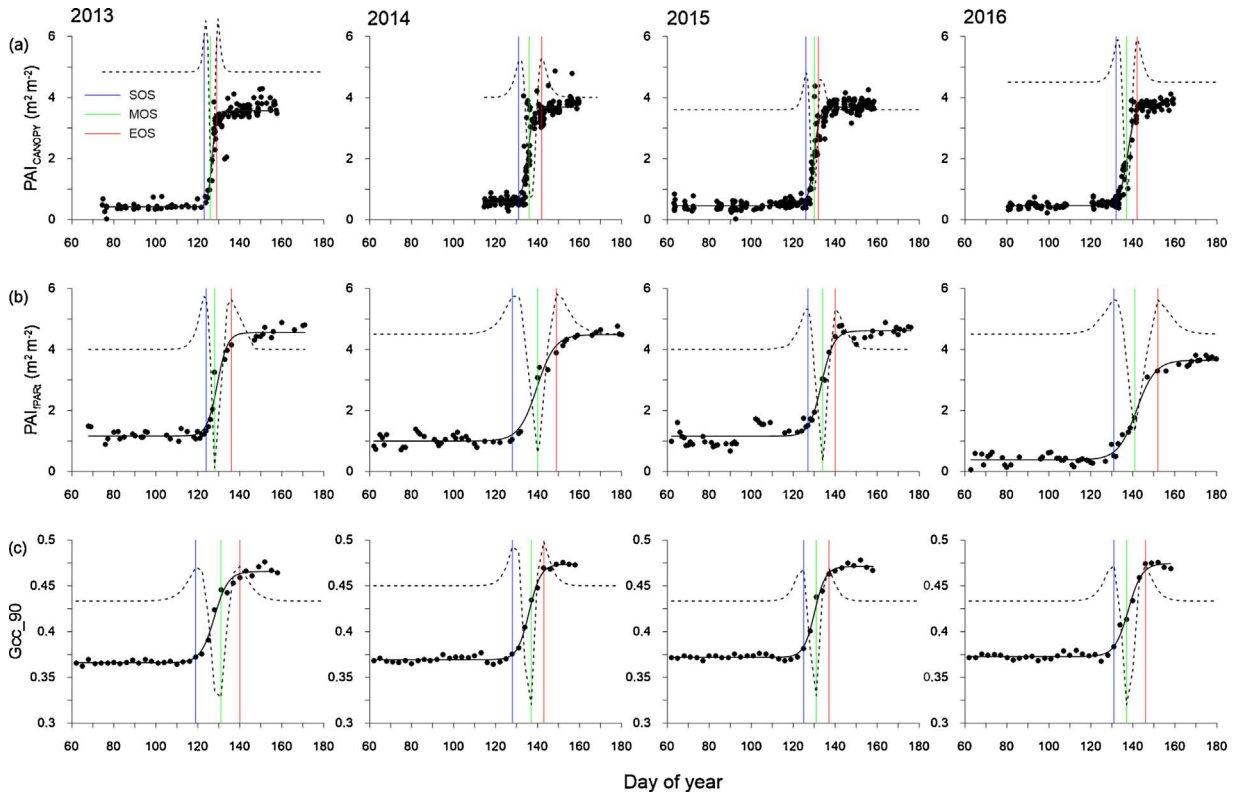

Fig. 3. Phenological transition dates in spring derived from the vegetation indices (VIs) (a) PAI_{CC} (upper), (b) PAI_{fTPAR} (middle), and (c) green chromatic coordinates (G_{CC}_90) (lower) from 2013 to 2016. Regarding the specific transition dates, the start of greening in spring (SOS) (blue line), middle of the phenological transition period in spring (MOS) (green line), and end of the completion of leaf unfolding (EOS) (red line) represent the start, middle, and end of spring, respectively. The dotted line denotes the rate of change of curvature for each VI, based on the method developed by Zhang et al. (2003), with transition dates (SOS, MOS, and EOS) determined based on curvature maxima/minima. The closed circle indicates the intended VI, and the solid line is the fit based on a non-linear fitting approach. (For interpretation of the references to colour in this figure legend, the reader is referred to the web version of this article.)

were mostly similar for SOA with the difference in about 5 days ahead or behind at a maximum, with 2014 generally being the earliest autumn, and 2015 the latest. As a consequence, the duration of the transition from SOA to EOA was longest for R_{CC}_90 (≈5-7 weeks), intermediate for G_{CC}_90 and PAI_{fPARt} (≈3-5 weeks), and shortest for PAI_{CANOPY} (≈1-3 weeks) (Table 1).

5. Discussion

5.1. Uncertainty of LAI from canopy cover images (LAI_{CANOPY})

We found the upward-looking camera-derived LAI_{CANOPY} showed the similar seasonal track to the PAR-derived LAI_{fPARt} throughout a year in 4 years, although LAI_{CANOPY} was marginally lower than LAI_{fPARt} during the full-leaf period. In the Bartlett Experimental Forest, Zhao et al. (2011) compared the representative maximum PAIs (i.e., effective LAIs) in July during the plant growth season obtained based on several observations: litter-trap, fisheye photography, LAI-2000 plant canopy analyzer (Li-Cor, Inc.), and a narrow-band near-infrared LIDAR technique that characterized the vertical distribution of foliage. They determined PAIs of 3.6–5.0 $m^2\,m^{-2}$, and found that the PAIs obtained from the litter trap and hemispherical fisheye images tended to be on the lower end of this range, while that those from the LAI-2000 and LIDAR tended to be on the upper end of this range. We calculated summertime PAIs of ≈3.5–4 $m^2\,m^{-2}$ using canopy cover images, and ≈4–5 $m^2\,m^{-2}$ from fractional PAR measurements. Hence, the absolute estimates of PAI, and the variation among approaches, as reported by Zhao et al. (2011) are comparable to our results.

There are still unknown concerns about what caused the difference in LAI between the different approaches. During the peak growing season, both LAI_{CANOPY} and LAI_{fPARt} varied from day-to-day by up to about 1 $m^2\,m^{-2}$. However, there were systematic differences between the approaches in that in 2013, 2014 and 2015, LAI_{CANOPY} tended to be about 0.5 $m^2\,m^{-2}$ lower than LAI_{fPARt} (in 2016 the difference was near-zero). Obviously, given the heterogeneous canopy cover, differences in the exact location at which instruments were installed is one explanation.

But, several other sources of uncertainty for the LAI_{CANOPY} estimates might also be considered. One potential uncertainty is the effect of the automatic exposure setting on the calculated LAI_{CANOPY}. Most of the canopy cover images taken during the full-leaf period were overexposed as a consequence of canopy closure due to dense foliage. In such dense canopy conditions, the DRP approach with automatic exposure generally yields lower PAI, and thus lower LAI compared to other methods. Macfarlane et al. (2011) compared changes in frequency histograms of blue channel in canopy images with the different photographic exposures, and found that increase in exposures creates brighter images, and the maximum frequency of sky pixels shifted further to the right, increasing the mixed pixels in the histogram of blue channel. However, the maximum frequency of canopy pixels was less affected by increasing exposures. As a result, increasing exposure by one stop reduced the calculated LAI by 9–12% (Macfarlane et al., 2011). As shown in 4.1, in the present study, the difference in maximum LAI_{CANOPY} and LAI_{fPARt} averaged approximately 0.3 $m^2\,m^{-2}$, indicating less than 10% of both maximum LAI_{CANOPY} and LAI_{fPARt}. Accordingly, this suggests that the slight difference could have been reduced further with optimal camera exposure settings: Macfarlane et al. (2014) recommend using uncompressed, RAW format (rather than JPEG) files and underexposing images by one stop, although this is not an option with the camera we used.

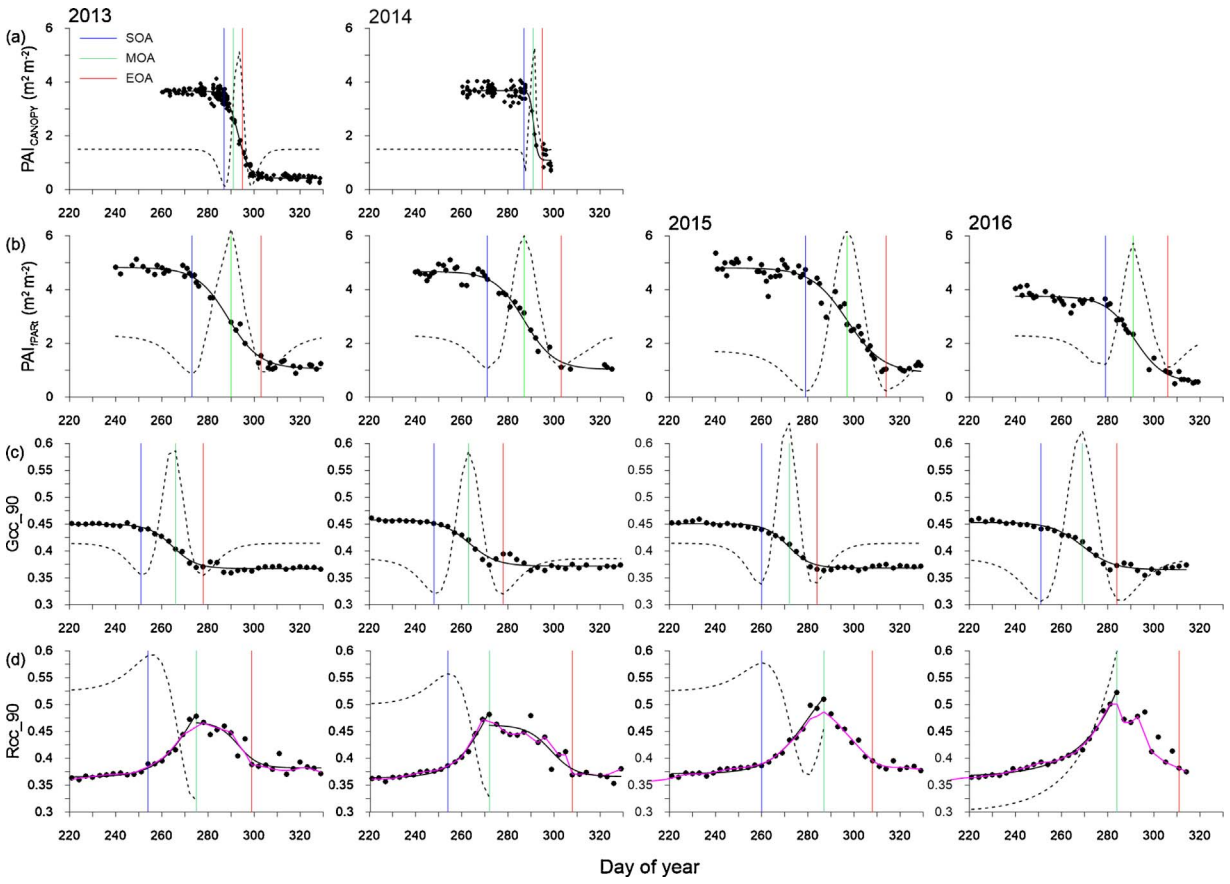

Fig. 4. Phenological transition dates in autumn derived from the VIs (a) PAI_{CC} (upper), (b) PAI_{fTPAR} (upper-middle), (c) G_{CC}_90 (lower-middle), and red chromatic coordinates (R_{CC}_90) (lower) from 2013 to 2016. Regarding the specific transition dates, SOA, MOA and EOA represents the start, middle, and end of autumn, respectively. The dashed line denotes the rate of change of curvature for each VI, based on the method developed by Zhang et al. (2003), with transition dates determined based on curvature maxima/minima. The closed circle indicates the intended vegetation index, and the black solid line is the fit based on a non-linear fitting approach. For (d), the solid line is likewise used to estimate SOA and EOA, whereas, for estimating EOA, the magenta solid line is the fit based on the smoothing and interpolation method using the local regression approach. (For interpretation of the references to colour in this figure legend, the reader is referred to the web version of this article.)

An additional concern may be associated with the threshold given in the present algorithm, which is used to allocate the mixed pixels existing in the blue channel of each image into canopy or sky elements (see Eqs. (1) and (2)). We changed the originally established 25% threshold in Eq. (1) to 40%, and 60%, which produces large allocation of the mixed pixels into the canopy elements, and examined the calculations to assess the difference in LAI_{CANOPY} as affected by these thresholds using the imagery data in 2013. The result yielded subtle increase in LAI_{CANOPY} by 2% ($2.95 \pm 1.37\ m^2\ m^{-2}$) for 40% ($P < 0.1$), and 4% ($3.01 \pm 1.41\ m^2\ m^{-2}$) for 60% ($P < 0.001$) thresholds, respectively, representing less impact of the different thresholds of mixed pixels on LAI_{CANOPY} estimates (data not shown) because the frequency of histogram in the mixed pixels is relatively smaller in each image (Fig. 1).

Other sources of uncertainty in optical LAI measurements have been assessed by Richardson et al. (2011), who estimated, based on repeat measurements at the same sampling points, that random uncertainty in measured LAI using optical devices was 10% or less, while systematic errors associated with instrument calibration and data processing might be on the order of 10–20%. Sampling uncertainty itself was also estimated to be small, provided that a sufficient number ($n = 20$ or more) of measurement points was used. Here, we used only a single measurement point for LAI_{CANOPY}, so sampling uncertainties alone are undoubtedly substantial.

5.2. Evaluations of LAI (LAI_{fPARt}) from radiometric PAR measurements

In contrast to LAI_{CANOPY}, LAI_{fPARt} uses simultaneous measurements of incident (above-canopy) and transmitted (below-canopy) PAR. This method appears to be highly sensitive to fine changes in canopy structure, including leaf development (Fig. 2). However, a concern remains regarding how well the spatial variability in the transmitted light below the canopy can be observed. In this study, we assumed that the stand was composed of a randomly distributed but spatially homogeneous arrangement of individual trees (with no large gaps that could generate a large variance between PAR measurements from the four equipped quantum sensors) and used the mean PAR of the four measurements (Jenkins et al., 2007). Ideally, more sensors would be used to capture the below-canopy light variability more precisely, given the fact that at least $n = 20$ litter traps should be equipped at the target site to obtain satisfactory total litter fall with an acceptable standard error (e.g., Newbould, 1967; Proctor et al., 1983). Indeed, the advantage of the measuring leaf area with portable instruments such as the LAI-2000 canopy analyzer, or LIDAR equipment, is that it is possible to sample in one day a large number points distributed throughout the forest, enabling more accurate evaluation of LAI at the stand level. However, repeating this sampling to obtain detailed phenological information is challenging. Thus while a limited number of instruments deployed in fixed locations, as with the quantum sensors used for PAI_{fPARt} together with the digital camera used for PAI_{CANOPY}, may not produce accurate estimates of the absolute amount of leaf area, they greatly facilitate tracking of phenology at a fine temporal scale.

5.3. Comparison of transition dates among the different metrics

From the comparison of the PAI time series between the different approaches together with the additional vegetation indexes of G_{CC}_90 and R_{CC}_90, PAI_{fPARt} showed smooth increase in PAI during the transition phase in spring until the maximum PAI, and also smooth decrease from the maximum PAI in autumn, respectively (Fig. 2). For PAI_{CANOPY}, the transition phases in spring and autumn occurred during a shorter time interval compared to the time courses of PAI_{fPARt}, and G_{CC}_90, and R_{CC}_90 (Figs. 3 and 4, Table 1). This suggests that the canopy cover DRP approach might have failed to track subtle change in PAI, or might have saturated at relatively low amounts of leaf area, because of the camera's autoexposure setting. The timing of SOS from PAI_{CANOPY} was consistent with those of PAI_{fPARt} and G_{CC}_90, while, for the timing of EOA, PAI_{CANOPY} was closer to PAI_{fPARt} compared to G_{CC}_90. We believe that PAI_{CANOPY} is most sensitive to changes in canopy structure when PAI is low, e.g. the dynamics associated with the onset of leaf opening, or the completion of leaf fall. Therefore, the canopy cover images appropriately capture the foliage timings with regard to these events. By comparison, PAI_{CANOPY} is relatively insensitive to changes in canopy structure when PAI is high, and thus it is more difficult to track the actual progression of green-up in spring or senescence in autumn, and so EOS and SOA derived from PAI_{CANOPY} may be less useful than the corresponding dates obtained using either the PAI_{fPARt} or G_{CC}_90.

An additional VI, G_{CC}_90 yielded similar transition dates and length in spring compared to the above and below canopy PAR measurements, capturing fine and gradual dynamics in colors due to spring bud break and leaf opening. However, in previous studies, it has been pointed out that because of the viewing geometry, the phenocam imagery tends to emphasize vegetation that is closest to the camera, and suggested that because of the oblique view, the effective leaf area is enhanced (Keenan et al., 2014). This may result in a failure to track fine and gradual dynamics in greenness, in turn yielding a faster transitional phase. For instance, Yang et al. (2013) suggested that spring peak of G_{CC} was earlier than the peak of total chlorophyll concentration in leaf. However, the consistency of transition dates between G_{CC}_90 and PAI_{fPARt} suggests that both metrics are similarly responsive to pronounced structural changes in the canopy that are associated with budburst and leaf expansion.

In contrast to the spring transitions, the extended period of autumn transitions can be attributed to the gradual coloration and senescence of the canopy. In this study, SOA from R_{CC}_90 was consistent with that from G_{CC}_90, while MOA from R_{CC}_90 roughly lined up with EOA from G_{CC}_90 (Figs. 2 and 3; Table 1). Sonnentag et al. (2012) noted that R_{CC}_90 was a better indicator than G_{CC}_90 for identifying the timing, intensity and duration of autumn colors in forests dominated by deciduous species. However, because G_{CC} and R_{CC} are the product of both the amount of leaf area and the color of individual leaves, phenologic metrics derived from these vegetation indices are bound to differ from those, such as PAI_{CANOPY} or PAI_{fPARt}, that are not sensitive to leaf color—especially in autumn. This means that in autumn G_{CC} and R_{CC} are unable to serve as direct measures of leaf area, and explains why the transition dates derived from these indices differed from those derived from the canopy cover images and PAR measurements that were sensitive to structural changes in the canopy.

6. Concluding remarks

The estimated phenological metrics of the PAI and transition dates were compared using the 4 years' worth of data and several VIs obtained continuously, using optical methods, from a representative hardwood forest in Northeastern United States. Based on the results, the growth-period LAI derived from canopy cover images and above and below canopy radiometric PAR measurements were in the same range as previous results obtained using various methods (Jenkins et al., 2007; Zhao et al., 2011). However, the VIs applied in this study produced slightly different transition dates. In particular, the evaluated transition dates and lengths in autumn exhibited large differences among the VIs of PAI_{CANOPY}, G_{CC}, R_{CC} and PAI_{fPARt}. These differences are presumably attributable to the specific vegetation statuses detected by each VI. Thus the most appropriate indicator clearly depends on the specific phenological parameter of interest.

We found that LAI estimated from simultaneous above and below canopy PAR measurements provided better representation of the seasonal dynamics of leaf area than LAI estimated from canopy cover imagery, which suffered from the effects of automatic exposure. Likewise, vegetation indices that were sensitive to leaf color, i.e. G_{CC} and R_{CC}, did not represent the trajectory of leaf area in autumn. Thus we conclude that the PAR measurements provide better overall indicator of LAI and phenological transition date estimations obtained from long-term monitoring measurements in the cool-temperate hardwood forest. However, the drawbacks we found with canopy cover imagery might be rectified with a different model of camera and different camera settings (Macfarlane et al., 2014). Because canopy cover imagery provides a permanent visual record of the state of the canopy, there is certainly merit in pairing this approach with radiometric measurements.

In conclusion, long-term overall operations from a multi-sensor approach, integrating with above and below canopy PAR measurements, will result in reduced uncertainty in estimates of phenological transition dates and the trajectory of canopy development and senescence, and will thus contribute to improved understanding of the biological controls on forest-atmosphere exchanges of energy, water, and carbon.

Acknowledgements

We appreciate two anonymous reviewers who gave invaluable suggestions for this paper. We would like to express an appreciation to Prof. Macfarlane, Prof. Younryel Ryu, and Prof. Sachinobu Ishida who gave us technical advice for digital image processing. MT acknowledges financial support from the Global COE program (principal investigator, Prof. Yasuhiro Yamanaka) by the Ministry of Education, Culture, Sports, Science and Technology and by Hiroshima University. ADR acknowledges support from the National Science Foundation's Macrosystems Biology (awards EF-1065029 and EF-1702697) and LTER (award DEB-1114804) programs, and the Northeastern States Research Cooperative. Research at Bartlett Experimental Forest is supported by the USDA Forest Service's Northern Research Station. We really thank to Prof. Takashi Kohyama for numerous supports of the present research.

References

Chianucci, F., Cutini, A., 2013. Estimation of canopy properties in deciduous forests with digital hemispherical and cover photography. Agric. For. Meteorol. 168, 130–139.
Ellwood, E.R., Temple, S.A., Primack, R.B., Bradley, N.L., Davs, C.C., 2013. Record-breaking early flowering in the eastern United States. PLoS One 8, e53788.
Fu, Y.H., Zhao, H., Piao, S., Peaucelle, M., Peng, S., Zhou, G., Ciais, P., Huang, M., Menzel, A., Peñuelas, J., Song, Y., Vitasse, Y., Zeng, Z., Janssens, I., 2015. declining global warming effects on the phenology of spring leaf unfolding. Nature 526, 104–108.
Hufkens, K., Friedl, M.A., Keenan, T.F., Sonnentag, O., Bailey, A., O'keefe, J., Richardson, A.D., 2012. Ecological impacts of a widespread frost event following early spring leaf-out. Global Change Biol. 18, 2365–2377.
Ide, R., Oguma, H., 2010. Use of digital cameras for phenological observations. Ecol. Inf. 5, 339–347.
Jenkins, J.P., Richardson, A.D., Braswell, B.H., Ollinger, S.V., Hollinger, D.Y., Smith, M.-L., 2007. Refining light-use efficiency calculations for a deciduous forest canopy using simultaneous towe-based carbon flux and radiometric measurements. Agric. For. Meteorol. 64–79, 143.
Keenan, T.F., Darby, B., Felts, E., Sonnentag, O., Freidl, M.A., Hufkens, K., O'Keefe, J., Klosterman, S., Munger, J.W., Toomey, M., Richardson, A.D., 2014. Tracking forest phenology and seasonal physiology using digital repeat photography: a critical assessment. Ecol. Appl. 24, 1478–1489.
Keenan, T.F., 2015. Spring greening in a warming world. Nature 526, 48–49.
Klosterman, S.T., Hufkens, K., Gray, G.M., Melaas, E., Sonnentag, O., Lavine, I., Mitchell, L., Norman, R., Friedl, M.A., Richardson, A.D., 2014. Evaluating remote sensing of

deciduous forest phenology at multiple statial scales using PhenoCam imagery. Biogeosciences 11, 4305–4320.
Kucharik, C.J., Norman, J.M., Gower, S.T., 1999. Characterization of radiation regimes in nonrandom forest canopies: theory, measurements, and a simplified modeling approach. Tree Physol. 19, 695–706.
Leblanc, S.G., Chen, J.M., Fernandes, R., Deering, D.W., Conley, A., 2005. Methodology comparison for canopy strucure parameters extraction from digital hemispherical photography in boreal forests. Agric. For. Meteorol. 129, 187–207.
Leblanc, S.G., 2004. Digital Hemispherical Photography Manual, Draft Version 1.0 (17 September 2004). Canada Centre for Remote Sensing, Natural Resouces, Canada, Ottawa.
Linkosalmi, M., Aurela, M., Tuovinen, J.-P., Peltoniemi, M., Tanis, C.M., Arslan, A.N., Kolari, P., Böttcher, K., Aalto, T., Rainne, J., Hatakka Juha Laurila, T., 2016. Digital photography for assessing the link between vegetation phenology and CO_2 exchange in two contrasting northern ecosystems. Geosci. Instrum. Method. Data Syst. 5, 417–426.
Ma, X., Huete, A., Yu, Y., Restrepo-Coupe, N., Beringer, J., Hutley, L.B., Kanniah, K.D., Cleverly, J., Eamus, D., 2014. Parameterization of an ecosystem light-use-efficiency model for predicting savanna GPP using MODIS EVI. Remote. Sens. Env. 154, 253–271.
Macfarlane, C., Hoffman, M., Eamus, D., Kerp, N., Higginson, S., McMurtrie, R., Adams, M., 2007. Estimation of leaf area index in eucalypt forest using digital photography. Agric. For. Meteorol. 143, 176–188.
Macfarlane, C., Ryu, Y., Ogden, G.N., Sonnentag, O., 2014. Digital canopy photography: exposed and in the raw. Agric. For. Meteorol. 197, 244–253.
Macfarlane, C., 2011. Classification method of mixed pixels does not affect canopy metrics from digital images of forest overstorey. Agric. For. Meteorol. 151, 833–840.
Newbould, P.J., 1967. Methods for estimating the primary production of forests. IBP Handbook. Blackwell Sci. Publ, Oxford, pp. 62.
Peñuelas, J., Rutishauser, T., Filella, I., 2009. Phenology feedbacks on climate change. Science 324, 887–888.
Pekin, B., Macfarlane, C., 2009. Measurement of crown cover and leaf area index using digital cover photography and its application to remote sensing. Remote Sens. 1, 1298–1320.
Primack, R.B., Gallinat, A.S., 2016. Spring budburst in a chaging climate. Am. Sci. 104, 102–109.
Primack, R.B., 2014. Walden Warming, Climate Change Comes to Thoreau's Woods. The University of Chicago Press Chicago, pp. 266.
Proctor, J., Anderson, J.M., Fogden, S.C.L., Vallack, H.W., 1983. Ecological studies in for contrasting lowland rain forests in Gunung Mulu national park, Sarawak: II. litterfall, litter standing crop and preliminary observations on herbivory. J. Ecol. 71, 261–283.
Richardson, A.D., Jenkins, J.P., Braswell, B.H., Hollinger, D.Y., Ollinger, S.V., Smith, M.-L., 2007. Use of digital webcam images to track spring green-up in a deciduous broadleaf forest. Oecologia 152, 323–334.
Richardson, A.D., Braswell, B.H., Hollinger, D.Y., Jenkins, J.P., Ollinger, S.V., 2009. Near-surface remote sensing of spatial and temporal variation in canopy phenology. Ecol. Appl. 19, 1417–1428.
Richardson, A.D., Dail, D.B., Hollinger, D.Y., 2011. Leaf area index uncertainty estimates for model-data fusion applications. Agric. For. Meteorol. 151, 1287–1292.
Richardson, A.D., Anderson, R., Arain, M.A., Barr, A.G., Bohrer, G., Chen, G., Chen, J.M., Ciais, P., Davis, K.J., Desai, A., Dietze, M.C., Dragoni, D., Garrity, S.R., Gough, C.M., Grant, R., Hollinger, D.Y., Margolis, H.A., Mccaughey, H., Migliavacca, M., Monson, R.K., Munger, W., Pooulter, B., Raczka, B.M., Ricciuto, D.M., Sahoo, A.K., Schaefer, K., Tian, H., Vargas, R., Verbeeck, H., Xiao, J., Xue, Y., 2012. Terrestrial biosphere models need better representation of vegetation phenology: results from the North American carbon program site synthesis. Global Change Biol. 18, 566–584.
Richardson, A.D., Keenan, T.F., Migliavacca, M., Ryu, Y., 2013a. Climate change, phenology, and phenological control of vegetation feedbacks to the climate system. Agric. For. Meteorol. 169, 156–173.
Richardson, A.D., Klosterman, S., Toomey, M., 2013b. Near-Surface sensor-derived phenology. In: Schwarts, M.D. (Ed.), Phenology: An Integrative Environmental Science. Springer. http://dx.doi.org/10.1007/978-94-007-6925-0_22.
Rosin, P.L., 2001. Unimodal thresholding. Pattern Recogn. 34, 2083–2096.
Ryu, Y., Sonnentag, O., Nilson, T., Vargas, R., Kobayashi, H., Wenk, R., Baldocchi, D.D., 2010. How to quantify tree leaf area index in an open savanna ecosystem: a multi-instrument and multi-model approach. Agric. For. Meteorol. 150, 63–76.
Ryu, Y., Verfaillie, J., Macfarlane, C., Kobayashi, H., Sonnentag, O., Vargas, R., Ma, S., Baldocchi, D.D., 2012. Continuous observation of tree leaf area index at ecosystem scale using upward-pointing digital cameras. Remote Sens. Environ. 126, 116–125.
Sonnentag, O., Hufkens, K., Teshera-Sterne, C., Young, A.M., Friedl, M., Braswell, B.H., Milliman, T., O'Keefe, J., Richardson, A.D., 2012. Digital repeat photography for phenological research in forest ecosystems. Agric. For. Meteorol. 152, 159–177.
Toomey, M., Friedl, M., Frolking, S., Hufkens, K., Klosterman, S., Sonnentag, O., Baldocchi, D.D., Bernacchi, C.J., Biraud, S.C., Bohrer, G., Brzostek, E., Burns, S.P., Coursolle, C., Hollinger, D.Y., Margolis, H.A., McCaughey, H., Monson, R.K., Munger, J.W., Pallardy, S., Phillips, R.P., Torn, M.S., Wharton, S., Zeri, M., Richardson, A.D., 2015. Greenness indices from digital cameras predict the timing and seasonal dyanmics of canopy-scale photosynthesis. Ecol. Appl. 25, 99–115.
Turner, D.P., Urbanski, S., Bremer, D., Wofsy, S.C., Meyers, T., Gower, S.T., Gregory, M., 2003. A cross-biome comparison of daily light use efficiency for gross primary production. Global Change Biol. 9, 383–395.
Yang, X., Tang, J., Mustard, J.F., 2013. Beyond leaf color: comparing camera-based phenological metrics with leaf biochemical biophysical, and spectral properties throughout the growing season of a temperate deciduous forest. J. Geophys. Res. Biogeosci. 119, 181–191.
Zhang, X., Friedl, M.A., Schaaf, C.B., Strahler, A.H., Hodges, J.C.F., Gao, F., Reed, B.C., Huete, A., 2003. Monitoring vegetation phenology using MODIS. Remote Sens. Environ. 84, 471–475.
Zhao, F., Yang, X., Schull, M.A., Román-Colón, M.O., Yao, T., Wang, Z., Zhang, Q., Jupp, D.L.B., Lovell, J.L., Culvenor, D.S., Newnham, G.J., Richardson, R.D., Ni-Meister, W., Schaaf, C.L., Woodcock, C.E., Strahler, A.H., 2011. Measuring effective leaf area index, foliage profile, and stand height in New England forest stands using a full-waveform ground-based lidar. Remote Sens. Environ. 115, 2954–2964.